Heat Flux on EAST Divertor Plate in H-mode with LHCD/LHCD+NBI *

Bo Shi(史博)[1,2,3], Zhen-Dong Yang(仰振东)[4], Bin Zhang(张斌)[1], Cheng Yang(杨程)[1], Kai-Fu Gan(甘开福)[1], Mei-Wen Chen(陈美文)[1], Jin-Hong Yang(杨锦宏)[3], Hui Zhang(张辉)[3], Jun-Li Qi(祁俊力)[3], Xian-Zu Gong(龚先祖)[1], Xiao-Dong Zhang(张晓东)[1], Wei-Hua Wang(汪卫华)[1,3]**

[1]*Institute of Plasma Physics, Hefei Institutes of Physical Sciences, Chinese Academy of Sciences, Hefei 230031*
[2]*Science Island Branch of Graduate School, University of Science and Technology of China, Hefei 230031*
[3]*Institute of Applied Physics, Army Officer Academy, Hefei 230031*
[4]*Teaching and Research Department of Physics, Tongling University, Tongling 244000*

(Received 17 March 2017)

Based on the surface temperature measured by the infrared camera on the experimental advanced superconducting tokamak (EAST), the heat fluxes on the lower outer divertor target plate during H-mode with the lower-hybrid wave current drive (LHCD) only and with the LHCD combined with the neutral beam injection (NBI) are calculated by the DFLUX code and compared. The analyzed discharges are lower single null divertor configuration discharges. In the case with the LHCD only ($I_p \sim 400\,kA$, $P_{LHCD} \sim 2\,MW$), ELM-free appears after L-H transition with the peak heat flux on the lower outer target plate less than $1\,MW/m^2$. However, there is no ELM-free appearing after the L-H transition in the case with the LHCD+NBI ($I_p \sim 300\,kA$, $P_{LHCD} + P_{NBI} \sim 2\,MW$). The results show that the peak heat fluxes on the lower outer target plate in the LHCD+NBI H-mode cases are larger than those in the LHCD H-mode under the similar auxiliary heating power. This is because the heat flux profiles of the lower outer target plate as a function of plate location in ELMing with the LHCD+NBI are narrower than those with the LHCD only. The results are consistent with the results in terms of the scrape-off layer width observed in the EAST.

PACS: 52.55.Fa, 52.55.Rk DOI: 10.1088/0256-307X/34/9/095201

One of the characteristics of H-mode discovered in 1982 on the ASDEX is the ELMs accompanied with periodicity,[1] which is the process of collapse rebuilt of the edge transport barrier. H-mode with the ELM plasma regime is considered to be a preferable scenario in the future fusion devices such as ITER. ELMs have the advantage that they expel the impurity from the core plasma, but the disadvantage that the transient and repetitive particle and heat loads are deposited on the divertor.[2] Thus one of the largest threats to tokamaks is from repetitive heat and particle expulsion events which damage divertor plates by melting and evaporation and thus limit the life of divertor tiles.[3,4] ELMs have been classified into several types: type I, type Ⅱ, type Ⅲ, compound and other types. When the heating power exceeds 1.5–2 times the L-H threshold power, the type-I ELM H-mode regime is usually obtained. It suddenly releases typically 5–30% of the pedestal stored energy in a time scale of a few hundreds of μs, and most of the resulting high heat fluxes are deposited on the divertor target plates.[5]

EAST is a fully superconducting tokamak with ITER-like configuration and heating scheme, which has a flexible poloidal field control system to accommodate both the single null (SN) and the double null (DN) divertor configurations.[6,7] It has the upgraded tungsten upper divertor based on cassette and mono block technology and the lower divertor remained carbon in 2014,[8,9] and lithium coating has been proven to be the most effective wall conditioning technology employed in EAST.[6] EAST has achieved an H-mode duration record over 60 s in the 2016 experimental campaign. The LHCD (2.45 GHz and 4.6 GHz) systems, the ion cyclotron resonant heating (ICRF) systems, the electron cyclotron resonant heating (ECRH) systems, and the NBI system are all equipped in EAST.

The width of scrape-off layer (SOL) is an essential parameter to determine the peak heat flux on divertor target plates. The results on the EAST and the DⅢ-D have shown that the radio-frequency (RF)-heated plasma has a broader SOL than neutral beam (NB)-heated plasma when the edge electrons are effectively heated in low plasma current and low density regime with low edge collisionality.[7,10] To show the effect of the heating scheme on the heat flux of the divertor target plate intuitively, this work presents the study of heat fluxes on the lower outer target plate in H-mode with LHCD only and with LHCD+NBI in EAST. A brief introduction of the infrared (IR) diagnostic and heat flux calculation method, the results and analyses, and summary are given in the following.

An IR/visible endoscope system was built on EAST to monitor the lower divertor, upper divertor and limiter between P and N windows in 2014, which can acquire the IR and visible data simultaneously. The IR camera is a Flir SC7700BB. The IR range is 2.5–5.4 μm, and the frame rate is from 115 Hz

*Supported by the National Natural Science Foundation of China under Grant Nos 11505290, 51576208 and 11575239, and the National Magnetic Confinement Fusion Science Program of China under Grant Nos 2013GB113004 and 2015GB102004.
**Corresponding author. Email: whwang@ipp.ac.cn

(640 × 512 pixel) to 2.9 kHz (132 × 3 pixel). The spatial resolution of the camera is 4 mm on the divertor target plate. The observation area of the IR/visible system on EAST is shown in Fig. 1.

The temperature distributions on the lower outer target plate were measured by the IR camera. Then the heat flux distributions and the peak heat fluxes were calculated with a 2D finite element analysis code named as DFLUX, which provides the flexibility to specify the heat transmission coefficient for a loosely bound plasma-facing layer to reduce the influence of the unknown deposited layer on the calculation results. A basic description of the method is presented in the following, and more details can be found in Ref. [11]. The heat transmission coefficient defined as $\alpha = k_{\rm layer}/d_{\rm layer}$ is used as a boundary condition when calculating with the measured evolution of the surface temperature, where $k_{\rm layer}$ represents the heat conduction behavior of the unknown deposited layer and $d_{\rm layer}$ is the layer thickness.[12,13] The heat fluxes are two-dimensional results calculated by taking a line in the radial direction on the lower outer target plate from the IR data, with the endpoint of the line is the joint of the dome and the outer target plate. It also has the flexibility to select the line according to the measured results and toroidal symmetry is assumed. Thus the peak heat fluxes of the divertor target plate and the heat flux profiles as a function of plate location can also be acquired.

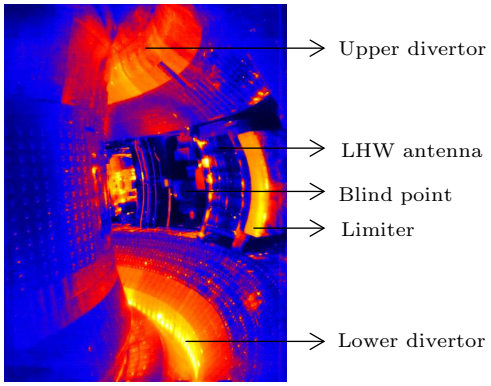

Fig. 1. The observation area of the IR/visible system.

The analyzed discharges were lower single null (LSN) divertor configuration discharges. Researchers have shown that the radial transport across the separatrix during ELMs originates predominantly from the low-field-side (LFS), resulting in the parallel transport from the LFS to the high-field-side (HFS) in the LSN limited by the presence of the secondary X-point. Therefore, the heat fluxes on the lower outer target plate are calculated only in this study. The heat fluxes during ELMs are ELMing-averaged results if the frequency of ELMing is more than 115 Hz, as the frequency of the IR camera is set as 115 Hz.

Figure 2 shows the time evolution of some parameters and the peak heat flux on the lower outer divertor of an LSN H-mode discharge achieved with LHCD only, with the plasma current $I_{\rm p} \sim 400$ kA, the line-averaged electron density $n_{\rm e} \sim 3\times10^{19}\,{\rm m}^{-3}$–$3.8\times10^{19}\,{\rm m}^{-3}$, $dR_{\rm sep} = -1.6$ cm ($dR_{\rm sep} = R_{\rm sep,L} - R_{\rm sep,U}$, with $R_{\rm sep,L}$ and $R_{\rm sep,U}$ being the lower and upper separatrix radii mapped to the LFS mid-plane), the source power of LHCD $P_{\rm LHCD} \sim 2$ MW, and the toroidal field $B_{\rm t} \sim 2.3$ T.

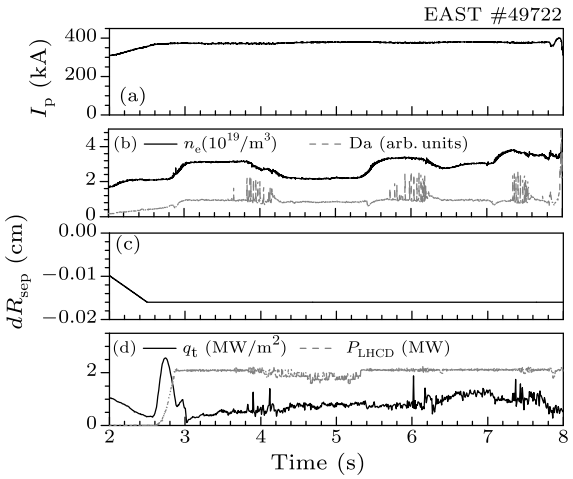

Fig. 2. (a) Plasma current, (b) plasma density and lower divertor D_α signal, (c) $dR_{\rm sep}$, and (d) source power of LHCD and peak heat flux on the lower outer divertor of discharge 49722.

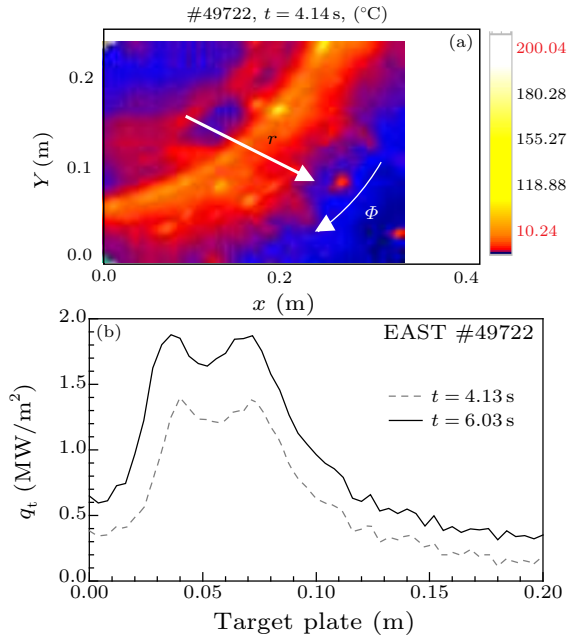

Fig. 3. (a) Surface temperature of lower outer target plate measured by the IR camera, and (b) heat flux profiles on the lower outer target plate as a function of plate location of discharge 49722.

When the LHCD started to work, the peak heat flux of the lower outer divertor varied rapidly. Unfortunately, the reason is not very clear. ELM-free occurred after L-H transition accompanied by the increasing electron density. The peak heat fluxes on the lower outer divertor during ELM-free were not more than 1 MW/m^2. Then ELMs appeared and $n_{\rm e}$ began to reduce and eventually lead to H-L transition. The

peak heat flux on the lower outer target plate during ELMs was not more than 2 MW/m^2.

Figure 3 shows the surface temperature of the lower outer target plate measured by the IR camera, and the heat flux profiles (ELMing-averaged heat fluxes) on the lower outer target plate as a function of plate location at $t = 4.13$ s and $t = 6.03$ s when peaks appear on the time trace of q_t in the discharge 49722. Here r represents the location on the divertor target, and Φ represents the toroidal direction. The coordinate origin in Fig. 3(b) is the joint of the dome and the outer target plate, and the abscissa is r. It can be seen that the heat flux curves are not single-peak structures, but wider curves.

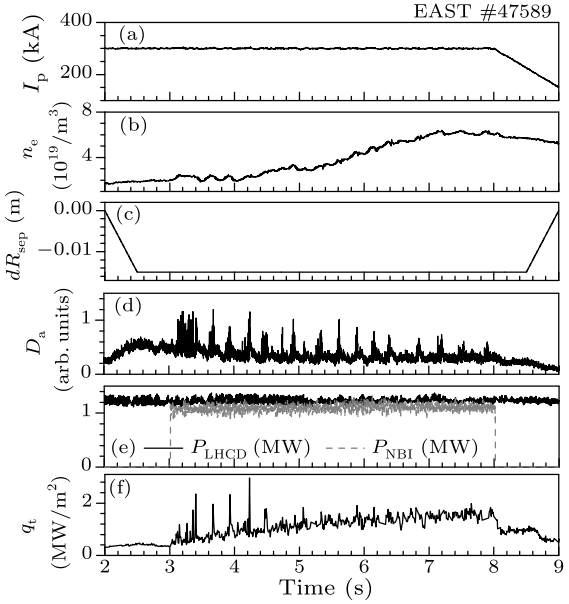

Fig. 4. (a) Plasma current, (b) plasma density, (c) dR_{sep}, (d) lower divertor D_α signal, (e) source power of LHCD and NBI, and (f) peak heat flux on the lower outer divertor of discharge 47589.

Figure 4 shows the time evolution of some parameters and the peak heat flux on the lower outer target plate of an LSN H-mode discharge achieved with LHCD+NBI, with the plasma current $I_p \sim 300$ kA, the line-averaged electron density $n_e \sim 2 \times 10^{19}$ m^{-3}–6.3×10^{19} m^{-3}, $dR_{sep} = -1.5$ cm, the source power of LHCD $P_{LHCD} \sim 1.2$ MW, the source power of NBI $P_{NBI} \sim 1$ MW, and the toroidal field $B_t \sim 2.3$ T.

In this case, the total power source including NBI and LHCD was about 2 MW, which is almost the same as that of the LHCD only, despite some differences from $I_p \sim 300$ kA, $dR_{sep} = -1.5$ cm. However, the heat flux characteristics are still very comparable. It can be seen that there is no ELM-free after L-H transition but ELMs occurring with n_e still increasing. The peak heat flux on the lower outer target plate during ELMs was about 3 MW/m^2 and ELMs disappeared when NBI was turned off. By comparing, it can be seen that the peak heat flux on the lower outer target plate during ELMs produced by NBI was larger and the characteristics are different from those produced by the LHCD.

Figure 5 shows the surface temperature of the lower outer target plate measured by the IR camera, and the heat flux profiles (ELMing-averaged heat fluxes) on the lower outer target plate as a function of plate location at $t = 3.93$ s and $t = 4.23$ s when peaks appear on the time trace of q_t in the discharge 47589. It can be seen that the heat flux curves are of single-peak structures. Both temperature distribution and heat flux curves are narrower compared with discharge 49722. There are some toroidal asymmetries that do not affect the result, as the typical areas were chosen.

The heat fluxes in several discharges were calculated using the IR data under two conditions: LHCD H-mode and LHCD+NBI H-mode. The heat flux profiles of ELMing (ELMing-averaged) as a function of the plate location are shown in Fig. 6. The black curves are the heat flux curves with LHCD ($I_p \sim 400$ kA, discharges 49720 and 49722) only. The gray curves are the heat flux curves with LHCD+NBI ($I_p \sim 300$ kA, discharges 47329, 47331, 47332 and 47589).

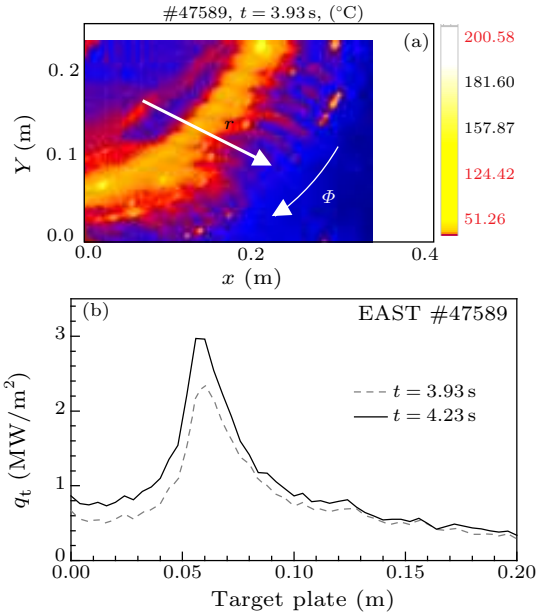

Fig. 5. (a) Surface temperature of the lower outer target plate measured by the IR camera, and (b) heat flux profiles on the lower outer divertor as a function of plate location of discharge 47589.

It can be seen that the gray curves are narrower compared with the black curves. This is the reason why the heat fluxes of the target plate during ELMs with LHCD+NBI are larger than those with LHCD only. The heat flux curves of the lower outer target plate as a function of the plate location by RF-heated are broader than those by NB-heated. The results are consistent with the SOL width results in EAST, which has shown that RF-heated plasma has a broader SOL than NB-heated plasma when the edge electrons are

effectively heated in low plasma current and low density regime with low edge collisionality.

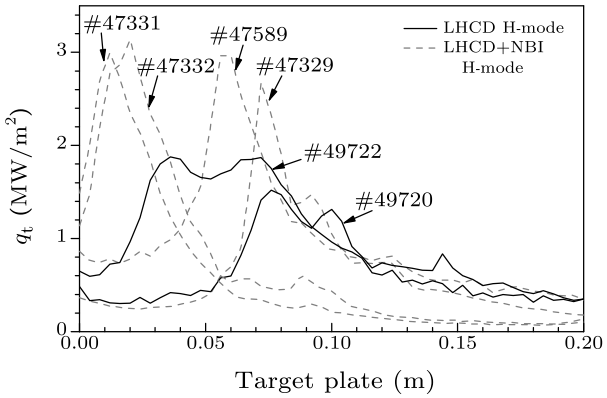

Fig. 6. Comparing heat flux profiles on the lower outer divertor as a function of the plate location.

In summary, heat fluxes on the lower outer target plate during H-mode with LHCD and with LHCD+NBI have been calculated and compared, aimed at studying the heat fluxes on the divertor target plate under different heating schemes.

The characteristics of the heat flux on the lower outer target plate during ELMs produced by LHCD+NBI are different from those produced by LHCD only. In the case with LHCD only ($I_p \sim 400\,\mathrm{kA}$, $P_{LHCD} \sim 2\,\mathrm{MW}$), ELM-free appears after L-H transition and is accompanied by the increasing electron density. The peak heat flux on the lower outer divertor during ELM-free is less than $1\,\mathrm{MW/m^2}$. Then ELMs appear and n_e begins to reduce, which eventually lead to H-L transition. The peak heat flux on the lower outer target plate during ELMs is less than $2\,\mathrm{MW/m^2}$ mostly. In the case of LHCD+NBI ($I_p \sim 300\,\mathrm{kA}$, $P_{LHCD} + P_{NBI} \sim 2\,\mathrm{MW}$), there is no ELM-free after L-H transition but ELMs appear with n_e still increasing. The peak heat flux on the lower outer target plate during ELMs is about $3\,\mathrm{MW/m^2}$ and ELMs disappear when NBI is turned off.

By comparing the heat flux profiles (ELMing-averaged heat fluxes) of the lower outer target plate as a function of plate location during ELMs, it can be seen that the heat flux curves with LHCD+NBI are narrower, consistent with the results on EAST that RF-heated plasma has a broader SOL width than NB-heated plasma when the edge electrons are effectively heated in low plasma current. This is the reason why the heat flux on the lower outer target plate during ELMs with LHCD+NBI is larger than that with LHCD only.

References

[1] Wagner F, Becker G and Behringer K 1982 *Phys. Rev. Lett.* **49** 1408
[2] Federici G, Skinner C H and Brooks J N 2001 *Nucl. Fusion* **41** 1967
[3] Wang L, Xu G S and Guo H Y 2012 *Nucl. Fusion* **52** 063024
[4] Ahn J W, Maingi R and Canik J M 2014 *Nucl. Fusion* **54** 122004
[5] Eich T, Herrmann A and Neuhauser J 2005 *Plasma Phys. Control. Fusion* **47** 815
[6] Wan B N, Li J G and Guo H Y 2013 *Nucl. Fusion* **53** 104006
[7] Wang L, Guo H Y and Xu G S 2014 *Nucl. Fusion* **54** 114002
[8] Zhou Z B 2015 *J. Fusion Energy* **34** 93
[9] Li W X, Song Y T and Ye M Y 2016 *J. Fusion Energy* **105** 15
[10] Wang L, Makowski M A and Guo H Y 2016 *22 International Conference on Plasma Surface Interactions in Controlled Fusion Device* (Rome, Italy May 30–June 3, 2016)
[11] Eich T, Andrew P and Herrmann A 2007 *Plasma Phys. Control. Fusion* **49** 573
[12] Gan K F, Li M H and Wang F M 2013 *J. Nucl. Mater.* **438** S364
[13] Zhang B, Gan K F and Gong X Z 2015 *Plasma Sci. Technol.* **17** 831